

www.acsami.org Research Article

Poly(Ethylene Glycol) Diacrylate as the Passivation Layer for High-Performance Perovskite Solar Cells

Wenzhan Xu,[†] Tao Zhu,[†] Haodong Wu, Lei Liu, and Xiong Gong*



Cite This: https://dx.doi.org/10.1021/acsami.0c11468



ACCESS

Metrics & More

Article Recommendations

ABSTRACT: In the past decade, greatest effect has been paid on organic—inorganic halide perovskites for approaching high-performance perovskite solar cells (PSCs). It was found that severe surface-defect within the perovskite active layer restricted further boosting device performance of PSCs. Here, we report high-performance PSCs by utilization of an ultrathin solution-processed poly(ethylene glycol) diacrylate (PEGDA) layer to passivate the surface-defect within the perovskite thin film. Systematical studies demonstrate that the PEGDA-passivated perovskite thin film exhibit suppressed nonradiative recombination and trap density, as well as superior film morphology with a smoother surface, larger crystal size, and better crystallinity. Moreover, PSCs by the PEGDA-passivated perovskite thin film

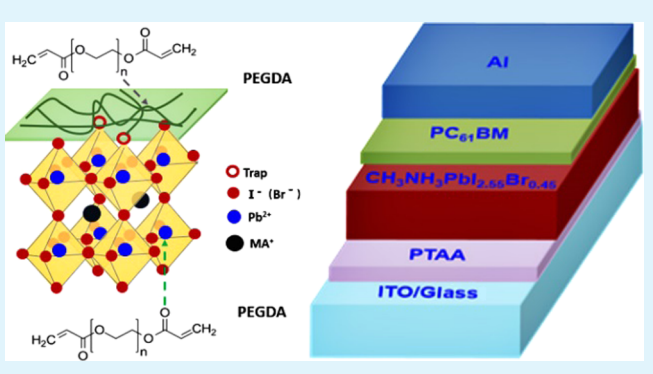


exhibit suppressed charge carrier recombination, reduced charge-transfer resistance, shorter charge carrier extraction time, and enlarged built-in potential. As a result, PSCs by the PEGDA-passivated perovskite thin film show a power conversion efficiency of over 21% and a photocurrent hysteresis index of 0.037. Moreover, unencapsulated PSCs by the PEGDA-passivated perovskite thin film possess over 10 day operational stability. All these results indicate that our approach provided a facile way to boost device performance of PSCs.

KEYWORDS: perovskite solar cells, power conversion efficiency, photocurrent hysteresis, surface-defect passivation, poly(ethylene glycol) diacrylate

■ INTRODUCTION

In the past decade, perovskite solar cells (PSCs) have been demonstrated to be an alternative cost-effective solar technology. 1-6 Over 25% power conversion efficiencies (PCEs) was reported by utilization of novel perovskite materials, manipulation of film morphologies of the perovskite active layer, construction of novel device architectures, and reengineering of the interfaces between the perovskite active layer and the electrodes. 6-9 Such an evolution dedicated great accomplishments, but the studies indicated that unbalanced charge carrier transport within the perovskite active layer, 10,11 severe charge carrier recombination induced by the surfacedefect, 12,13 and the trap states generated by counterions 14 restricted further boosting device performance of PSCs. Moreover, PSCs with a planar heterojunction (PHJ) rather than a mesoscopic (MS) device structure possesses great application potentials even if the highest PCEs were reported from PSCs with a MS device structure.6-9

Studies revealed that the vacancy, the interstitial defect, dislocation, and dangling bond within the surface of a perovskite thin film could serve as the centers for charge carrier recombination, which restricted charge carrier to be

transported and extracted efficiently, resulting in poor PCEs of PSCs. ^{14,15} Moreover, halide segregation-induced surface-defect was identified to be a serious issue for PSC degradation. ^{14–16} Many efforts have been devoted to passivate the surface-defect within solution-processed perovskite thin films for boosting the PCEs of PSCs. ^{17–19} Lewis acids and/or Lewis bases were utilized to passivate the PbX^{3–} and Pb²⁺ antisite defects within perovskite thin films. ^{20–22} Polymers were also used to reengineering the surface of solution-processed perovskite thin films for enhancing both PCEs and stabilities of PSCs. ^{23–25} For example, by utilization of a ultrathin solution-processed 4-lithium styrenesulfonic acid/styrene copolymer to passivate the surface-defect of a CH₃NH₃PbI₃ thin film, we observed high-performance (boosted efficient and stability) PSCs with dramatically suppressed photocurrent

Received: June 24, 2020 Accepted: September 11, 2020 Published: September 11, 2020



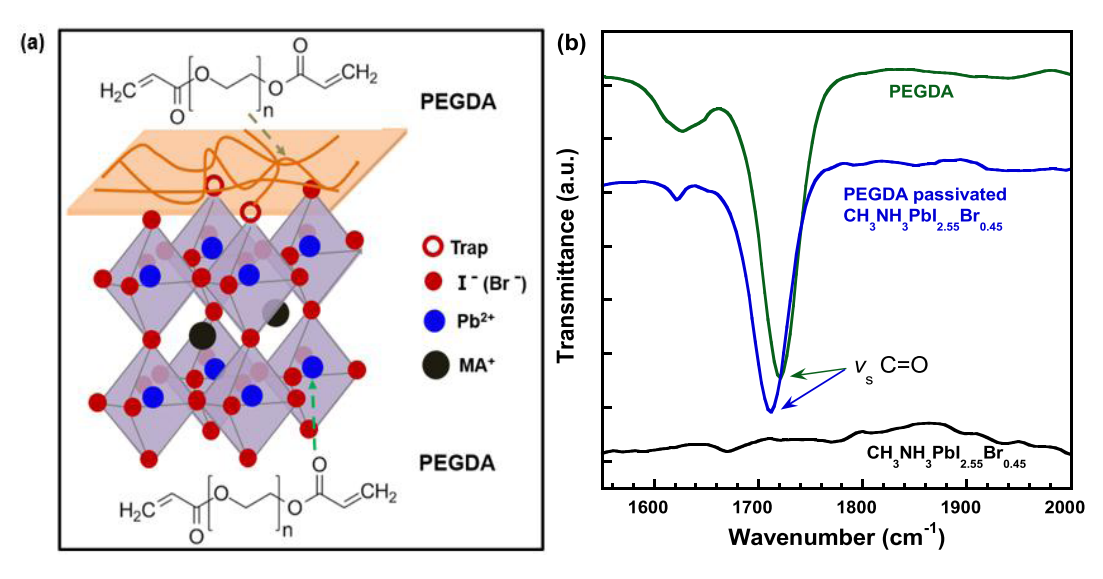


Figure 1. (a) Schematic illustration of the interaction of Pb and C=O (green dashed line represents Pb···C=O), and the potential surface defects passivation, (b) FTIR spectra of PEGDA, pristine CH₃NH₃PbI₂ 55Br_{0.45} thin film, and the PEGDA-passivated CH₃NH₃PbI₂ 55Br_{0.45} thin film.

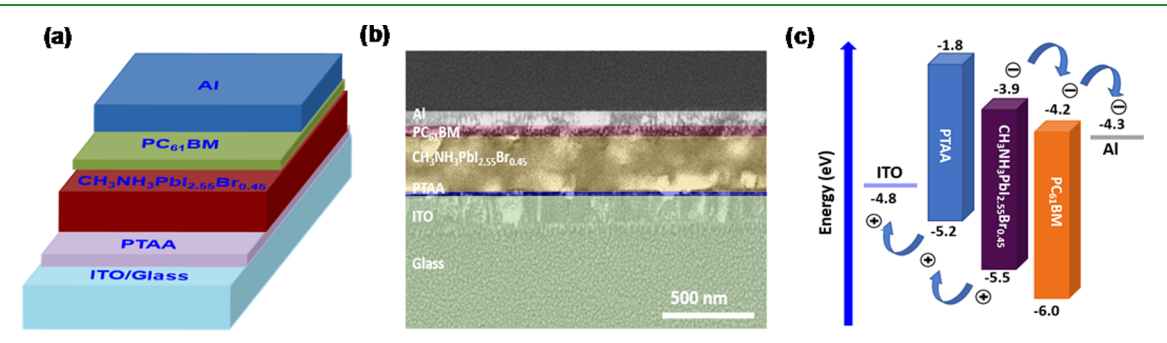


Figure 2. (a) PSC device structure, (b) cross-sectional SEM images of each layer in PSCs, (c) work functions of the ITO and Al electrodes, and the LUMO and HOMO energy levels of PTAA, $CH_3NH_3PbI_{2.55}Br_{0.45}$, and $PC_{61}BM$ thin films.

hysteresis. ²⁴ Lu et al. introduced poly(ethylene glycol) (PEG) to address unfully coverage of CsPbIBr₂ thin films on the TiO₂ layer and observed boosted a PCEs of 7.31%. ²⁶ Later on, You et al. systematically studied the influences of PEG on tuning the energy level and modifying the film morphology of the CsPbIBr₂ layer and revealed that the C–O–C bond could coordinate with CsPbIBr₂ to stabilize the α phase. ²⁷

In this study, we report high-performance (boosted efficiency and stability) PSCs with significantly suppressed photocurrent hysteresis through the utilization of an ultrathin solution-processed poly(ethylene glycol) diacrylate (PEGDA) layer to passivate the surface-defect within the solutionprocessed $CH_3NH_3PbI_{2.55}Br_{0.45}$ perovskite thin film. Studies indicate that the -C=O groups of PEGDA as the Lewis base can form an interaction with Pb2+ and therefore effectively passivate the surface-defect within the perovskite thin film. Further systemically studies demonstrate that the PEGDApassivated perovskite thin film possesses superior film morphology with a smooth surface, suppressed nonradiative recombination and trap density as well, enlarged crystal size, and enhanced crystallinity. Moreover, PSCs by the PEGDApassivated perovskite thin film exhibit suppressed charge carrier recombination, reduced charge-transfer resistance, shorter charge carrier extraction time, and enlarged built-in potential. As a result, PSCs by the PEGDA-passivated perovskite thin film exhibit 21.03% PCE with significantly reduced photocurrent hysteresis and boosted stability compared to the pristine perovskite thin film.

■ RESULTS AND DISCUSSION

Figure 1a schematically illustrates the proposed working mechanism of the CH₃NH₃PbI_{2.55}Br_{0.45} perovskite thin film passivated by PEGDA. PEGDA (molecular structure, inset of Figure 1a) possesses two -C=O groups, which could act as the Lewis base to passivate the surface-defect of perovskite thin films. 20,28 To verify the hypothesis as shown in Figure 1a, Fourier transform infrared (FTIR) spectroscopy is carried out to investigate chemical bonds between the PEGDA thin layer and the CH3NH3PbI2.55Br0.45 perovskite thin film, and the results are shown in Figure 1b. The stretching vibration of -C=O groups in PEGDA is peaked at 1728 cm⁻¹, whereas the stretching vibration of -C=O groups in the PEGDApassivated CH₃NH₃PbI_{2.55}Br_{0.45} thin film is shifted to 1711 cm⁻¹. However, no peak at this position is observed from the pristine perovskite thin film. The result demonstrated that the Lewis adduct (-C=O···Pb) is formed between the PEGDA thin layer and the CH₃NH₃PbI_{2.55}Br_{0.45} thin film, ^{20,28} which demonstrates that the surface-defect within the CH3NH3PbI2.55Br0.45 thin film is passivated by the PEGDA layer. Such passivation certainly suppresses surface charge carrier recombination, which leads boosted PCEs for PSCs.^{21,24,29}

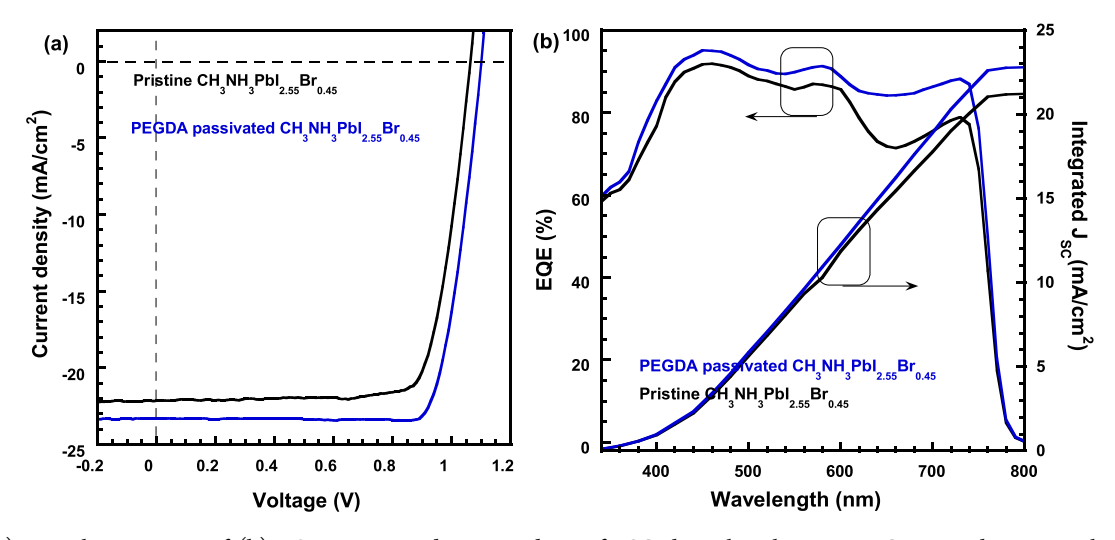


Figure 3. (a) J-V characteristics of (b) EQE spectra and integrated J_{SC} of PSCs by either the pristine CH₃NH₃PbI_{2.55}Br_{0.45} thin film or the PEGDA-passivated CH₃NH₃PbI_{2.55}Br_{0.45} thin film.

Table 1. Device Performance Parameters of PSCs

thickness of the PEGDA layer	$V_{\rm OC}$	Jsc	FF	PCE	R_{S}	R_{SH}
(nm)	(V)	$(mA cm^{-2})$	(%)	(%)	$(\Omega~\text{cm}^{-2})$	$\left(\Omega~cm^{-2}\right)$
0	$1.07 \ (1.05 \pm 0.02)$	$22.16 (20.82 \pm 0.67)$	$79 (76 \pm 3)$	$18.73 \ (17.54 \pm 1.19)$	16.45	854.51
3	$1.08 (1.07 \pm 0.01)$	$22.23 (21.35 \pm 0.54)$	$80 (77 \pm 3)$	$19.20\ (18.22\ \pm\ 0.98)$	14.42	962.18
5	$1.10 \ (1.09 \pm 0.01)$	$23.32 (22.42 \pm 0.38)$	$82 (80 \pm 2)$	$21.03 \ (20.14 \pm 0.89)$	6.35	1368.52
8	$1.09 \ (1.07 \pm 0.02)$	$22.21 (21.09 \pm 0.48)$	$81 (78 \pm 3)$	$19.61\ (18.78\ \pm\ 0.83)$	10.36	1243.36
12	$1.08 \ (1.06 \pm 0.02)$	$21.58 \ (20.32 \pm 0.62)$	$78 (75 \pm 3)$	$18.18 \ (17.04 \pm 1.14)$	20.17	534.54

^aPerformance metrics in parentheses are average values.

The photovoltaic properties of a PEGDA-passivated perovskite thin film are investigated and compared with a pristine perovskite thin film through PSCs with a device architecture of ITO/PTAA/perovskite/PC61BM/Al, as shown in Figure 2a, where ITO is indium tin oxide and serves as the anode, PTAA is poly[bis(4-phenyl)(2,4,6-trimethylphenyl)amine] and acts as the hole extraction layer (HEL), perovskite is either the PEGDA-passivated perovskite thin film or the pristine perovskite thin film, PC₆₁BM is phenyl-C₆₁-butyric acid methyl ester and serves as the electron extraction layer (EEL), and Al is aluminum and acts as the cathode, respectively. The crosssectional scanning electron microscopy (SEM) images of each layer within PSCs are displayed in Figure 2b. The perovskite photoactive layer is sandwiched by the PTAA HEL and the PC₆₁BM EEL. However, the PEGDA layer is too thin to be visibly observed in the cross-sectional SEM images without high resolution. Figure 2c displays the work functions (W_F) of the ITO and Al electrodes and the lowest occupied molecular orbital (LUMO) and the highest occupied molecular orbital (HOMO) energy levels of PTAA, perovskite, and PC₆₁BM thin films. The HOMO energy level (- 5.2 eV) of the PTAA HEL is aligned well with that (- 5.5 eV) of the $CH_3NH_3PbI_{2.55}Br_{0.45}$ layer and the W_F (- 4.8 eV) of the ITO anode. Such energy level alignment could ensure the separated holes to be transferred from the perovskite layer to the PTAA HEL and then being collected by the ITO anode. The LUMO energy level (-4.2~eV) of the PC₆₁BM EEL is well matched with the $W_{\rm F}$ (-4.3~eV) of the Al cathode, but is lower than that (- 3.9 eV) of the CH₃NH₃PbI_{2.55}Br_{0.45} layer. Such energy level alignment could also ensure the separated electrons being transferred from the CH₃NH₃PbI_{2.55}Br_{0.45} layer

into the PC₆₁BM EEL and then collected by the Al cathode. Thus, better device performance is anticipated from PSCs with a device architecture shown in Figure 2a.

Figure 3a presents the current density versus voltage (I-V)characteristics of PSCs, where PSCs are under the reverse scan direction (scan rate of 0.60 V s⁻¹) and illuminated with white light (AM 1.5G, 100 mW cm⁻²). PSCs with different device performance parameters are summarized in Table 1. The PSCs by the pristine perovskite thin film exhibit a short-circuit current (J_{SC}) of 22.16 mA cm⁻², an open-circuit voltage (V_{OC}) of 1.07 V, a fill factor (FF) of 79%, and with a corresponding PCE of 18.73%. These device performance parameters are consistent with those from PSCs with similar device structures. $^{30-33}$ The PSCs by the PEGDA (\sim 3 nm) passivated perovskite thin film exhibit a J_{SC} of 22.23 mA cm⁻², a V_{OC} of 1.08 V, a FF of 80%, and with a corresponding PCE of 19.20%. The PSCs by the PEGDA (~5 nm) passivated perovskite thin film exhibit a $J_{\rm SC}$ of 23.32 mA cm⁻², a $V_{\rm OC}$ of 1.10 V, a FF of 82%, and with a corresponding PCE of 21.03%. However, further increasing the thickness of the PEGDA passivation layer (~8 and ~12 nm), PSCs by the PEGDA-passivated perovskite layers exhibit decreased J_{SC} , V_{OC} , FF, and with the corresponding reduced PCEs.

The external quantum efficiency (EQE) spectra of PSCs by either pristine perovskite or PEGDA (\sim 5 nm) passivated perovskite thin films are shown in Figure 3b. It is found that PSCs by the PEGDA-passivated perovskite thin film reveals an enhancement in the EQE spectrum from 375 to 760 nm. The integrated $J_{\rm SC}$ from the EQE spectra are 21.72 and 22.93 mA cm⁻² for PSCs by the pristine perovskite thin film and PSCs by the PEGDA-passivated perovskite thin film, respectively. These

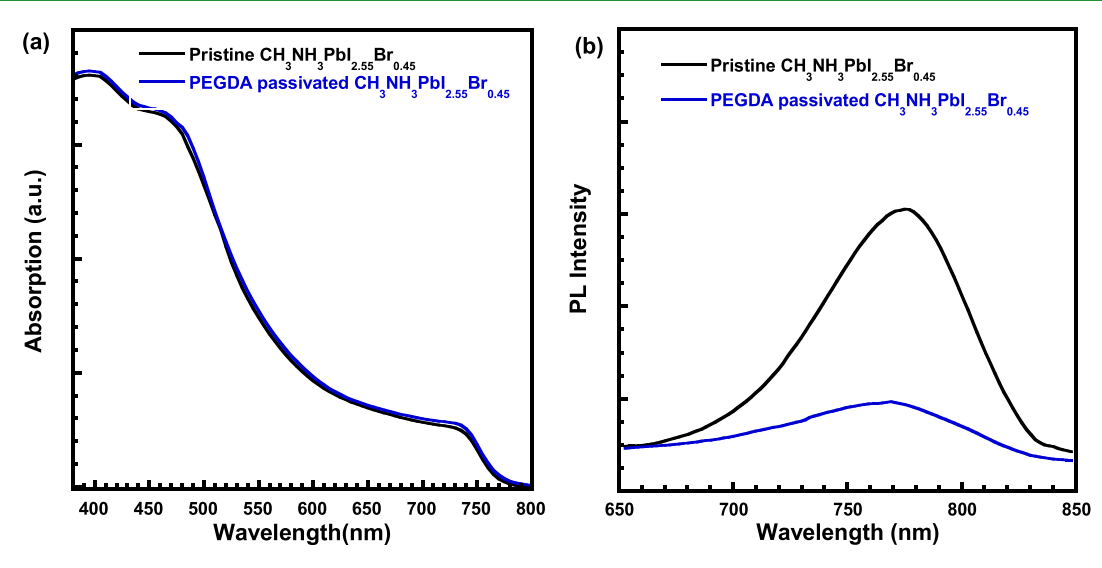


Figure 4. (a) Absorption spectra of the pristine $CH_3NH_3PbI_{2.55}Br_{0.45}$ thin film and the PEGDA-passivated $CH_3NH_3PbI_{2.55}Br_{0.45}$ thin film and (b) photoluminescence (PL) spectra of the pristine $CH_3NH_3PbI_{2.55}Br_{0.45}$ thin film and the PEGDA-passivated $CH_3NH_3PbI_{2.55}Br_{0.45}$ thin film coated on the top of the PTAA layer.

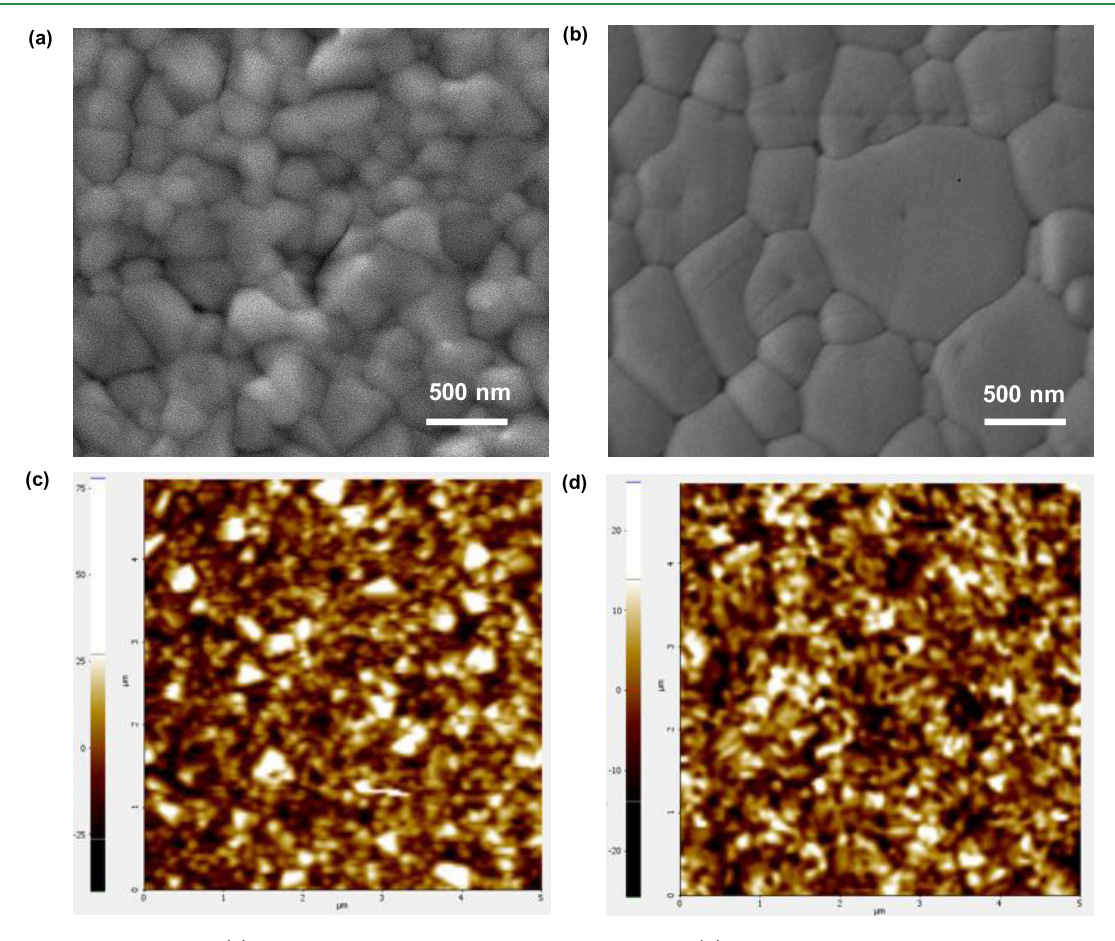


Figure 5. Top-view SEM images of (a) the pristine $CH_3NH_3PbI_{2.55}Br_{0.45}$ thin film and (b) the PEGDA-passivated $CH_3NH_3PbI_{2.55}Br_{0.45}$ thin film, and the AFM height images of (c) the pristine $CH_3NH_3PbI_{2.55}Br_{0.45}$ thin film and (d) the PEGDA-passivated $CH_3NH_3PbI_{2.55}Br_{0.45}$ thin film. All thin films are coated on the PTAA/ITO/glass substrates.

integrated J_{SC} values are consistent with those observed from the J-V characteristics (Figure 3a).

To explore the underlying physics of enhanced J_{SC} from PSCs by the PEGDA-passivated perovskite thin film, the absorption spectra of perovskite thin films are first performed. Figure 4a shows the absorption spectra of pristine perovskite

and PEGDA-passivated perovskite thin films. The negligible change observed from both absorption profiles demonstrates that the PEGDA passivation layer has no influence on the absorption of the perovskite thin film.

Figure 4b displays the photoluminescence (PL) spectra of pristine perovskite and PEGDA-passivated perovskite thin

ACS Applied Materials & Interfaces

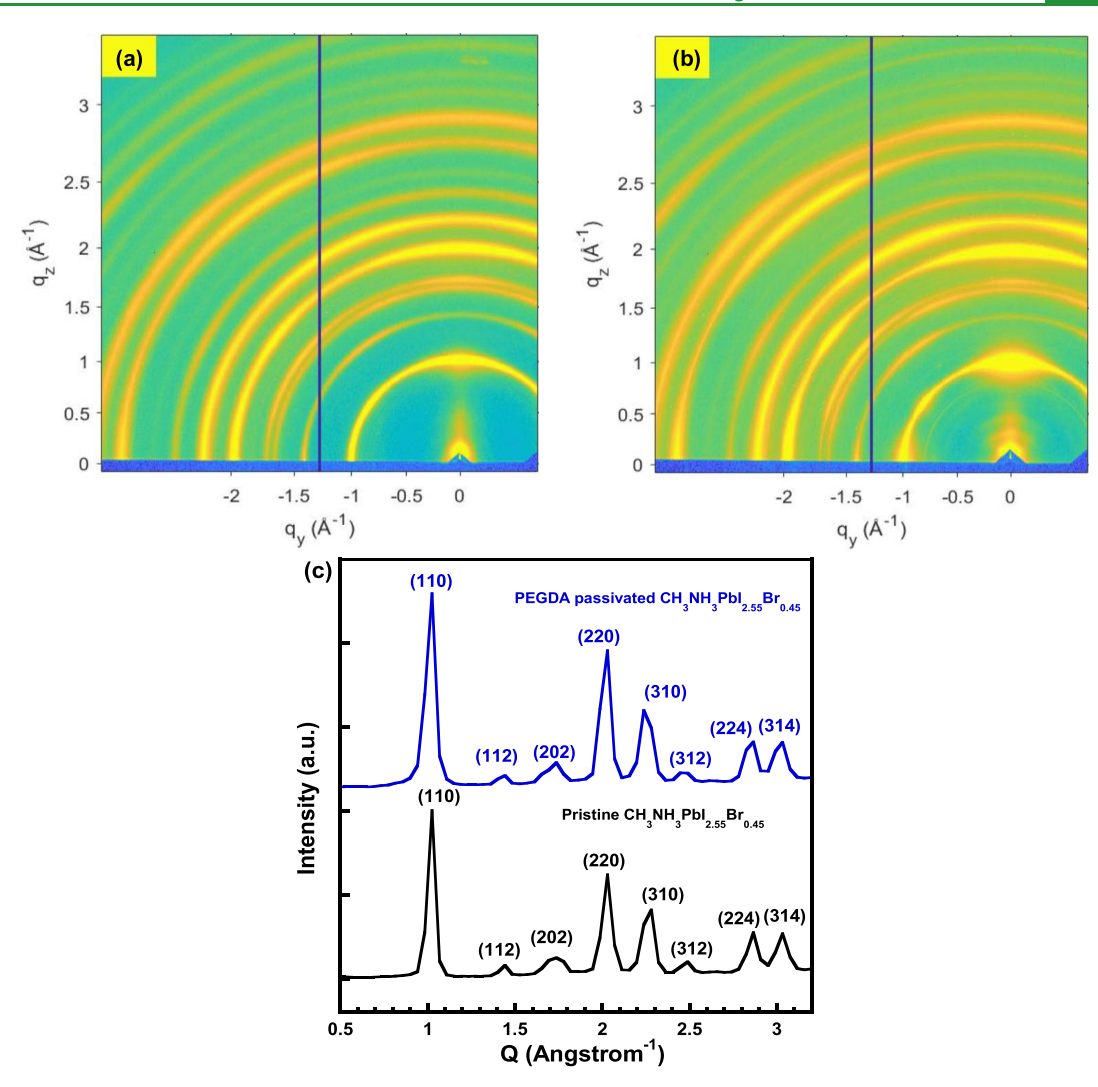


Figure 6. Two-dimensional (2D) grazing-incidence wide-angle X-ray scattering (GIWAXS) patterns of (a) the pristine $CH_3NH_3PbI_{2.55}Br_{0.45}$ thin film, (b) the PEGDA-passivated $CH_3NH_3PbI_{2.55}Br_{0.45}$ thin film, (c) one-dimensional (1D) GIWAXS patterns of the pristine $CH_3NH_3PbI_{2.55}Br_{0.45}$ thin film, and the PEGDA-passivated $CH_3NH_3PbI_{2.55}Br_{0.45}$ thin film.

films coated on the top of the PTAA layer. It is found that the PL intensity of the PEGDA-passivated perovskite thin film is reduced approximately 30% compared to the pristine perovskite thin film under the same condition. These results indicate that the PEGDA-passivated perovskite thin film possesses suppressed nonradiative recombination loss. Therefore, enhanced $J_{\rm SC}$, FF, and higher PCE are observed from PSCs by the PEGDA-passivated perovskite thin film.

Figure 5a,b displays the top-viewed SEM images of the pristine and PEGDA-passivated perovskite thin films, where both thin films are coated on the PTAA/ITO glass substrates. It is clear that both thin films are fully covered over the PTAA HEL layer. However, the film morphology of the PEGDA-passivated perovskite thin film is obviously different to that of the pristine perovskite thin film. As compared with the pristine perovskite thin film, the PEGDA-passivated perovskite thin film possesses enlarged grain sizes and more compact crystal grain with a smoother surface.

The height images of the pristine perovskite thin film and the PEGDA passivate perovskite thin film, measured by atom force microscopy (AFM), are shown in Figure 5c,d. The rootmean-square (RMS) observed from the PEGDA (~5 nm) passivated perovskite thin film is ~7.1 nm, whereas a RMS of

 \sim 13.7 nm is observed from the pristine perovskite thin film. A smoother surface observed from the PEGDA-passivated perovskite thin film would facilitate charge carrier to be efficiently transported from the perovskite thin film to the PC₆₁BM EEL and then collected by the Al cathode. As a result, PSCs by the PEGDA-passivated perovskite thin film have both enlarged $J_{\rm SC}$ and FF, thus boosted PCEs, while more PEGDA particles within the PEGDA-passivated perovskite thin film could reduce the photocurrent of PSCs because of its poor electrical conductivity. Thus, PSCs by the PEGDA-passivated perovskite thin film over an \sim 8 nm PEGDA passivation layer exhibit poor PCEs.

Figure 6a,b presents the grazing-incidence wide-angle X-ray scattering (GIWAXS) of film morphology and the crystallographic orientations of perovskite thin films. Strong scattering rings originated from the polycrystalline structures are observed from the pristine perovskite thin film and the PEGDA-passivated perovskite thin film, which indicate that the crystal structure of the perovskite thin film is not affected by the PEGDA passivation layer. However, stronger oriented perovskite crystal domains along the in-plane direction are observed from the PEGDA-passivated perovskite thin film compared to the pristine perovskite thin film. Such observation

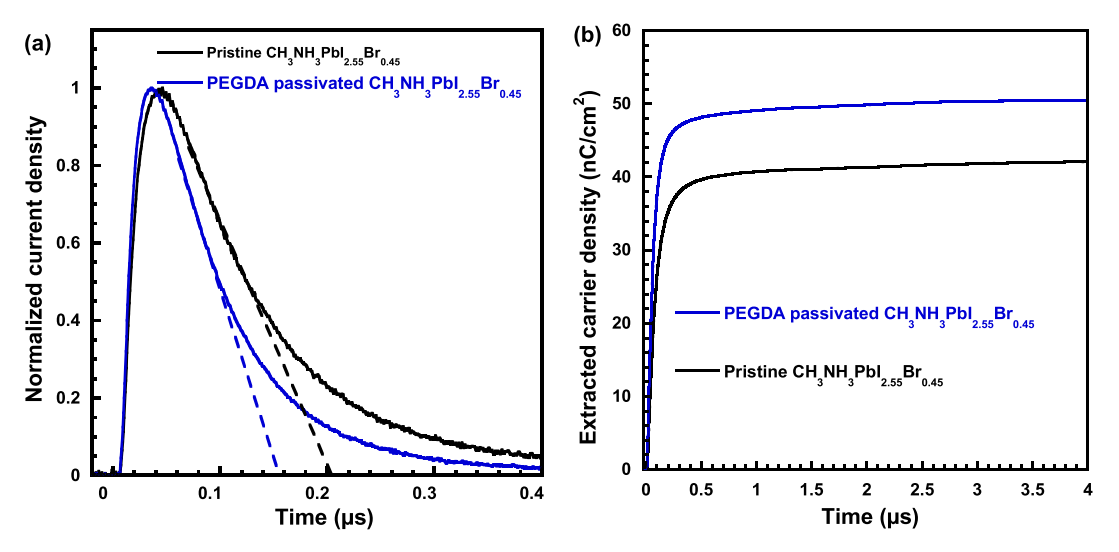


Figure 7. (a) Steady-state photocurrent output of (b) the extracted charge carrier densities of PSCs by either the pristine $CH_3NH_3PbI_{2.55}Br_{0.45}$ thin film or the PEGDA-passivated $CH_3NH_3PbI_{2.55}Br_{0.45}$ thin film.

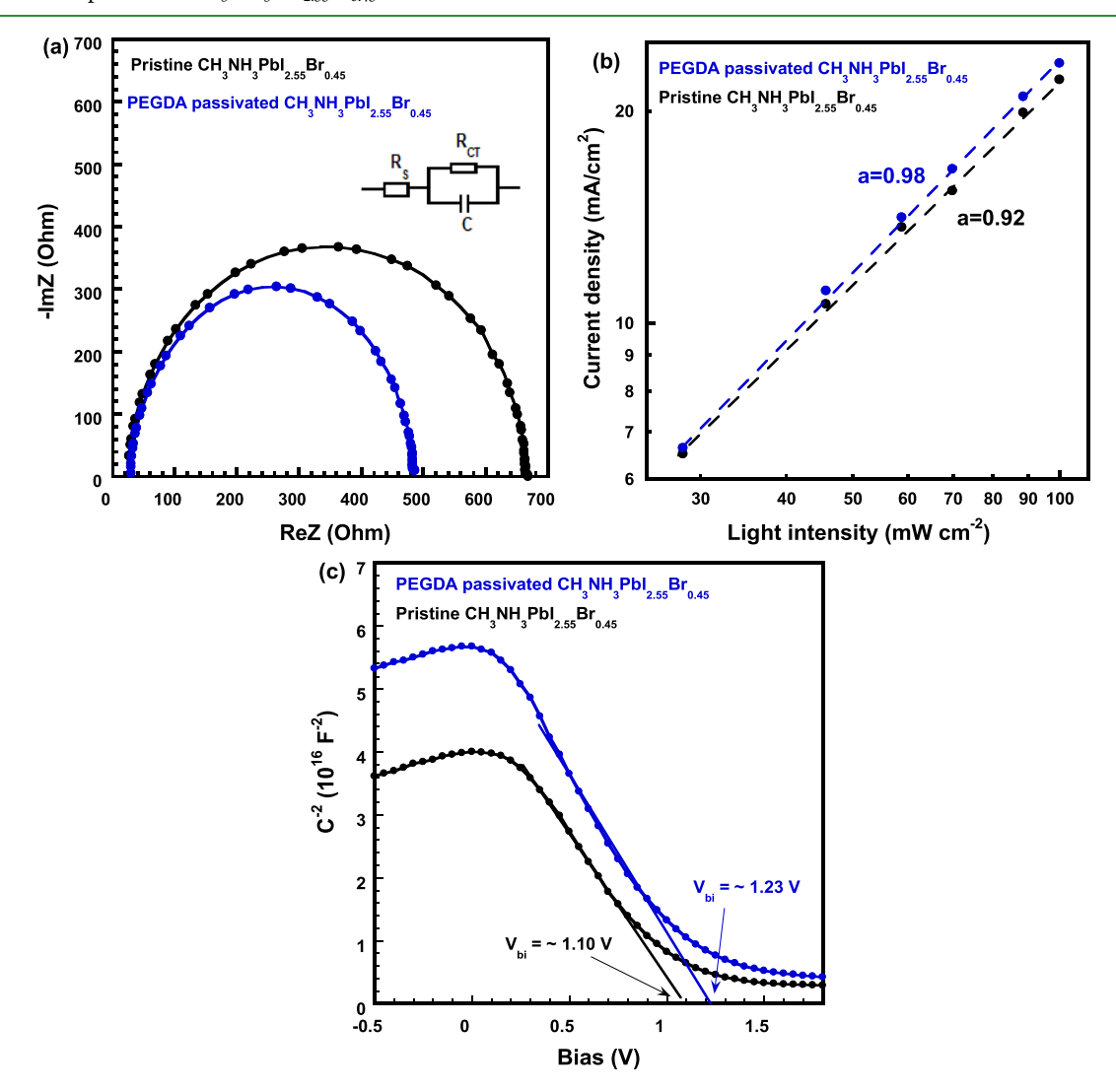


Figure 8. (a) Nyquist plots of and (b) the steady-state short-circuit current (the dotted lines represent fits to the expression $J_{SC} \propto I^a$) of and (c) the Mott–Schottky analysis for the interfacial trap densities and the built-in potentials of PSCs by either the pristine CH₃NH₃PbI_{2.55}Br_{0.45} thin film or the PEGDA-passivated CH₃NH₃PbI_{2.55}Br_{0.45} thin film. Inset (a) is the equivalent electric circuit, also called the RC circuit model.

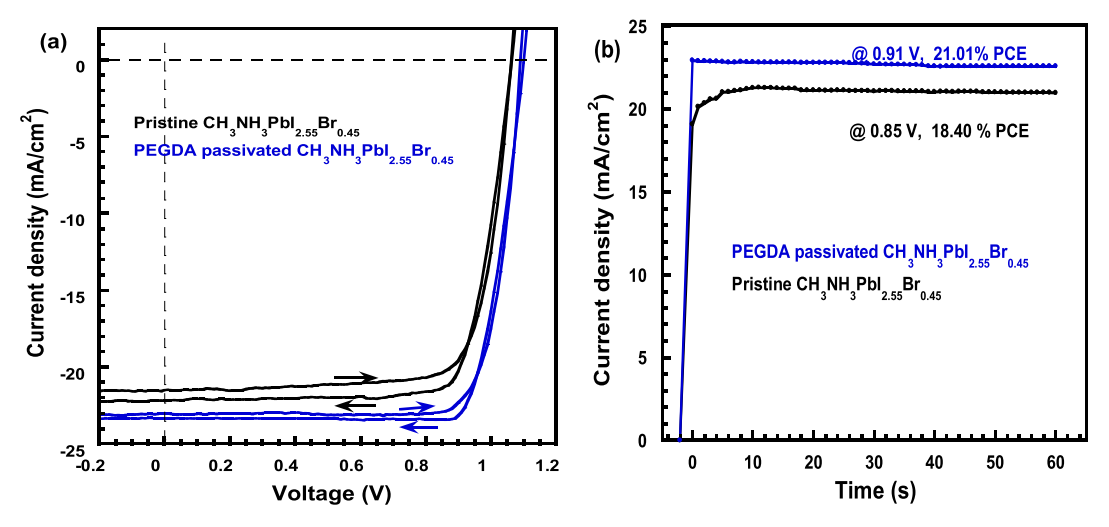


Figure 9. (a) J-V characteristics of and (b) steady-state photocurrent output of PSCs by either the pristine $CH_3NH_3PbI_{2.55}Br_{0.45}$ thin film or the PEGDA-passivated $CH_3NH_3PbI_{2.55}Br_{0.45}$ thin film.

demonstrates that more oriented and less amorphous perovskite crystal structures are formed in the PEGDA-passivated perovskite thin film. Thus, PSCs by the PEGDA-passivated perovskite thin film possess increased $J_{\rm SC}$ and enlarged FF, consequently enhanced PCEs.

Figure 6c presents the 1D GIWAXS patterns of two kinds of perovskite thin films. Eight major peaks, corresponding to the (110), (112), (202), (220), (310), (312), (224), and (314) lattice planes, respectively, are observed from both perovskite thin films, which indicate that both perovskite thin films have the tetragonal crystal structure. The Pegda intensities of the above eight lattice planes from the Pegda-passivated perovskite thin film are higher than those from the pristine perovskite thin film, demonstrating that the Pegda-passivated perovskite thin film possesses superior crystal domains. With such superior crystal domains, the charge carrier transporting within the Pegda-passivated perovskite thin film would be efficiently compared to the pristine perovskite thin film. As a result, PSCs by the Pegda-passivated perovskite thin film exhibit boosted PCEs.

The transient photocurrent (TPC) measurement is conducted to interpret charge carrier collection in PSCs^{30,36-39} Figure 7a presents the normalized TPC curves of PSCs under an applied voltage of -2 V. Under such high external voltage, all charge carriers should be separated rather than recombined. Thus, charge carrier transit time can be estimated by extrapolating the photocurrent in the linear region to zero point. 30,36-39 The charge carrier extraction times of ~210 nanoseconds (ns) and ~148 ns are observed from PSCs by the pristine perovskite thin film and PSCs by the PEGDA-passivated perovskite thin film, respectively. Such shorter charge carrier extraction time indicates that charge carrier extraction is efficiently within PSCs by the PEGDApassivated perovskite thin film. As a result, enhanced J_{SC} is observed from PSCs by the PEGDA-passivated perovskite thin film. Figure 7b presents the charge carrier densities, which are estimated by the integration of the transient photocurrent densities over the transient times. PSCs by the PEGDApassivated perovskite thin film possess approximatively 15% of the increased total charge carrier densities compared to the pristine perovskite thin film. This observation is consistent with device efficiency from the I-V characteristics as shown in

Figure 3a. Thus, PSCs by the PEGDA-passivated perovskite thin film exhibit boosted PCEs.

The impedance spectroscopy (IS) measurement is carried out to investigate the internal series resistances (R_s) of PSCs. ⁴⁰ $R_{\rm S}$ comprises the sheet resistance ($R_{\rm Sheet}$) of the electrodes and the charge-transfer resistance $(R_{\rm CT})$ at the interfaces between the electrodes (perovskite) and the charge carrier extraction layers. 41,42 Figure 8a shows the Nyquist plots of both PSCs. Both PSCs possess the same device structures and the only difference is the perovskite photoactive layer. Thus, the equivalent electric circuit (also called the RC circuit model) shown in the inset of Figure 8a is used to describe PSCs. 42 The semicircle in the Nyquist plots (Figure 8a) not only demonstrates that the RC circuit model is accurate but also indicates that each layer is relatively homogeneous along with the transport pathways without discernible multiple interfacial boundaries. ⁴¹ The $R_{\rm CT}$ value of PSCs by the pristine perovskite thin film is calculated to be \sim 668 Ω , which is larger than that (\sim 485 Ω) by the PEGDA-passivated perovskite thin film. This smaller $R_{\rm CT}$ is attributed to the superior film morphology and the smother surface of the PEGDA-passivated $CH_3NH_3PbI_{2.55}Br_{0.45}$ thin film.

The steady-state light intensity-dependent J_{SC} of PSCs are investigated for exploring underlying improved $J_{\rm SC}$ observed from PSCs by the PEGDA-passivated perovskite thin film. Figure 8b displays the steady-state J_{SC} versus the light intensity. In Figure 8b, the dotted lines represent fits to the expression $I_{SC} \propto I_{I}^{\alpha,43,44}$ where I is the light intensity and a is the coefficient, respectively. A near-linear dependence of J_{SC} with Ifor PSCs by the PEGDA-passivated perovskite thin film is observed, with a coefficient of $\alpha = 0.96$. In contrast, PSCs by the pristine perovskite thin film show a slightly nonlinear characteristics of J_{SC} versus I with $\alpha = 0.91$. Different α values indicate that different level nongeminate recombination processes take place in these two PSCs. A nearly linear dependence of J_{SC} with I indicates that the nongeminate recombination process is suppressed. ^{43,44} Therefore, PSCs by the PEGDA-passivated perovskite thin film exhibit enlarged I_{SC} and FF, and thus high PCE.

According to the Mott–Schottky analysis, 45,46 the built-in potentials $(V_{\rm bi})$ of PSCs can be estimated based on the capacitance–voltage (C-V) characteristics of PSCs. Figure 8c displays the C^{-2} versus V characteristics of PSCs. PSCs by the

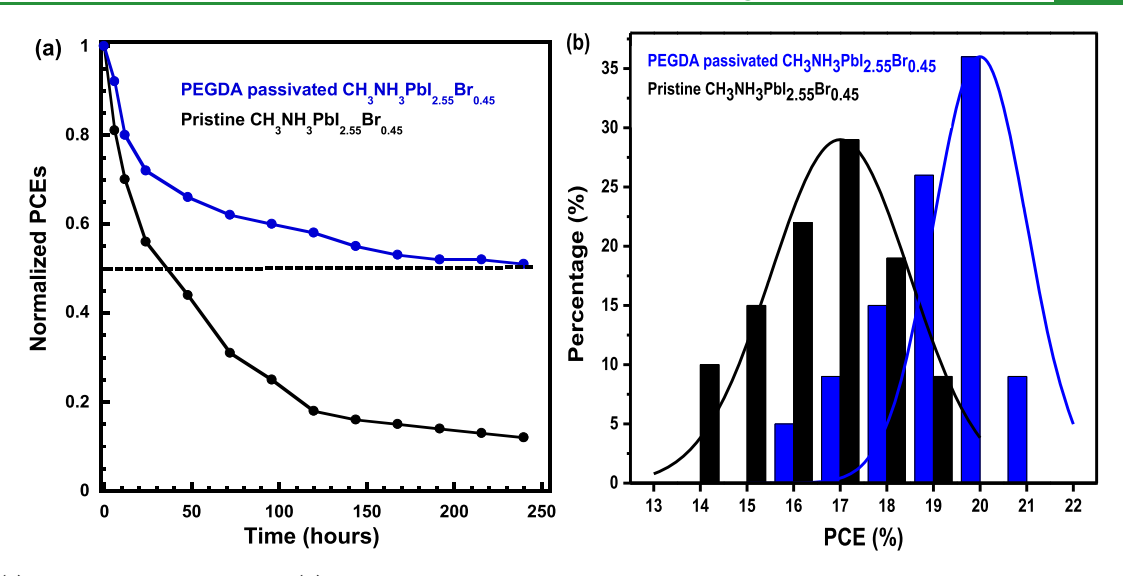


Figure 10. (a) Operational stability of and (b) histogram of power conversion efficiency of PSCs by either the pristine $CH_3NH_3PbI_{2.55}Br_{0.45}$ thin film or the PEGDA-passivated $CH_3NH_3PbI_{2.55}Br_{0.45}$ thin film.

pristine perovskite thin film exhibit a $V_{\rm bi}$ of ~1.10 V, which is smaller than that (~1.23 V) by the PEGDA-passivated perovskite thin film. As a result, PSCs by the PEGDA-passivated perovskite thin film exhibit a larger $V_{\rm OC}$ compared to the pristine perovskite thin film. Moreover, the slopes of the C^{-2} versus V characteristics for PSCs by the pristine perovskite thin film is calculated to be -4.62×10^{16} , which is also smaller than that (-7.53×10^{16}) by the PEGDA-passivated perovskite thin film. The larger absolute slope indicates the smaller interfacial charge carrier density within PSCs. ^{45,46} Thus, charge carrier recombination is suppressed in PSCs by the PEGDA-passivated perovskite thin film. ^{45,46} As a result, PSCs by the PEGDA-passivated perovskite thin film exhibit enhanced $J_{\rm SC}$, and consequently boosted PCEs.

With a scan rate of 0.6 V s^{-1} , the J-V characteristics of PSCs measured under different scan directions are shown in Figure 9a. It is clear that both PSCs exhibit different J-V curves, which indicate that PSCs possess the photocurrent hysteresis behaviors.⁴⁷ The photocurrent hysteresis is described as the hysteresis index (HI), which is defined as HI = (PCE_{reverse} -PCE_{forward})/PCE_{reverse}, where PCE_{reverse} and PCE_{forward} are the PCEs of PSCs measured under the reserve and forward direction, respectively. The HI is used to quantitatively describe the photocurrent hysteresis. The HI values for PSCs by pristine perovskite thin film and PSCs by the PEGDApassivated perovskite thin film are 0.053 and 0.037, respectively. Moreover, at a scan rate of 0.03 V s⁻¹, the HI values for PSCs by the pristine perovskite thin film and PSCs by the PEGDA-passivated perovskite thin film are 0.055 and 0.039, respectively. These results demonstrate that PSCs by the PEGDA-passivated perovskite thin film possess suppressed photocurrent hysteresis behaviors compared to the pristine perovskite thin film. Such suppressed photocurrent hysteresis behaviors are attributed to passivated surface-defect by the PEGDA thin layer, superior film morphology and more compact crystals with larger crystal sizes, and suppressed grain boundary induced by the PEGDA thin layer. 48-50 In addition, the weak hydrogen interactions between PEGDA and CH₃NH₃⁺ and/or I⁻ (Br⁻) within the perovskite thin film would restrict counterion migration, resulting in suppressed photocurrent hysteresis.47

Figure 9b shows the steady-state PCEs and photocurrent output as the function of time, where PSCs are performed under a constant bias, which closes to the maximum power point. PCEs of 18.40 and 21.01% are observed from PSCs by pristine perovskite thin film and PSCs by the PEGDA-passivated perovskite thin film, respectively. PSCs by the PEGDA-passivated perovskite thin film can instantly reach the steady-state current, but there is about 10 s delay for PSCs by the pristine perovskite thin film to reach the steady-state current. All of these results further reveal that PSCs by the PEGDA-passivated perovskite thin film possess suppressed photocurrent hysteresis behaviors compared to the pristine perovskite thin film.

Figure 10a shows the normalized PCEs as the function of time for both PSCs, where unencapsulated PSCs are under white light illumination with the light intensity of 100 mW cm⁻² in a glovebox with the nitrogen atmosphere. The PCEs of PSCs by the pristine perovskite thin film drop to the half of its initial value after 40 h. Under the same condition, the PCEs of PSCs by the PEGDA-passivated perovskite thin film maintains 50% of its initial value after 250 h. These results indicate that PSCs by the PEGDA-passivated perovskite thin film possess better stability compared to the pristine perovskite thin film.

The reproducibility of PSCs is further studied. The statistical PCE distributions of 40 devices for each type of PSCs are shown in Figure 10b. The PSCs by the PEGDA-passivated perovskite thin film show a good reproducibility with more than 80% PSCs with PCEs granter than 19%. It is clear that the deviation in PCEs observed from PSCs by the PEGDA-passivated perovskite thin film is much smaller than that by the pristine perovskite thin film. These results indicate that PSCs by the PEGDA-passivated perovskite thin film possess better reproducibility than that by the pristine perovskite thin film.

CONCLUSIONS

In summary, we reported high-performance PSCs with significantly suppressed photocurrent hysteresis by utilization of an ultrathin solution-processed PEGDA layer, which was functioned for the passivation layer to suppress the surface-defect within the solution-processed perovskite thin film. It was found that PEGDA as the Lewis base could form weak

interaction with Pb2+ and therefore effectively passivate the surface-defect within the perovskite photoactive layer. Systematical studies demonstrated that the PEGDA passivation layer could induce the perovskite thin film possessing a superior film morphology with a smooth surface, suppressed nonradiative recombination and trap density, enlarged crystal size, and enhanced crystallinity. Moreover, PSCs by the PEGDApassivated perovskite thin film exhibited reduced chargetransfer resistance, suppressed charge carrier recombination, reduced charge carrier extraction time, and enlarged built-in potential. As a result, as compared with PSCs by the pristine perovskite thin film, PSCs by the PEGDA-passivated perovskite thin film exhibited increased J_{SC} , enlarged V_{OC} and FF, with corresponding enhanced PCEs. Moreover, PSCs by the PEGDA-passivated perovskite thin film exhibited significantly decreased photocurrent hysteresis, boosted stability, and high reproducibility. All of these results demonstrated that our studies provided a simple way to approach PSCs with high performance.

EXPERIMENTAL SECTION

Materials. Lead iodide (PbI₂, 99.999%), poly[bis(4-phenyl)(2,4,6-trimethylphenyl)amine] (PTAA), anhydrous N,N-dimethylformamide (DMF, 99.8%), anhydrous ethanol (>99.5%), anhydrous toluene (99.8%), anhydrous chlorobenzene (CB, 99.8%), and poly(ethylene glycol) diacrylate (PEGDA) were purchased from Sigma-Aldrich. [6,6]-Phenyl-C61-butyric acid methyl ester (PC $_{61}$ BM, 99.5%) was purchased from Solenne BV. All materials were used as received without further purification. Methylammonium iodide (CH $_{3}$ NH $_{3}$ I (MAI)) and methylammonium bromide (MABr) were synthesized in our laboratory. $^{24,49-52}$

Preparation of Perovskite Precursor Solutions. PbI_2 , MAI, and MABr solutions were prepared as described in our previous publications. ^{24,49-52} Mixture MAI with MABr (85:15 by molar ratio) power was dissolved into the ethanol solvent to make a concentration of total 35 mg mL⁻¹ solutions.

Characterization of Perovskite Thin Films. All thin film characterizations have followed the methods described in our previous publications. $^{24,49-52}$

Fabrication and Characterization of PSCs. The procedures of PSC fabrication and characterization are the same as those reported in our previous publications. $^{24,49-52}$

AUTHOR INFORMATION

Corresponding Author

Xiong Gong — Department of Polymer Engineering, College of Polymer Science and Polymer Engineering, The University of Akron, Akron, Ohio 44325, United States; ⊚ orcid.org/0000-0001-6525-3824; Phone: (330)972 3406; Email: xgong@uakron.edu

Authors

Wenzhan Xu — Department of Polymer Engineering, College of Polymer Science and Polymer Engineering, The University of Akron, Akron, Ohio 44325, United States

Tao Zhu – Department of Polymer Engineering, College of Polymer Science and Polymer Engineering, The University of Akron, Akron, Ohio 44325, United States

Haodong Wu – Department of Polymer Engineering, College of Polymer Science and Polymer Engineering, The University of Akron, Akron, Ohio 44325, United States

Lei Liu — Department of Polymer Engineering, College of Polymer Science and Polymer Engineering, The University of Akron, Akron, Ohio 44325, United States

Complete contact information is available at:

https://pubs.acs.org/10.1021/acsami.0c11468

Author Contributions

[†]W.X. and T.Z. contributed equally to this work.

Notes

The authors declare no competing financial interest.

ACKNOWLEDGMENTS

The authors acknowledge the National Science Foundation (ECCS/EPMD 1903303) and Air Force Office of Scientific Research (AFOSR) (Grant number: FA9550-15-1-0292, Program Manager, Dr. Kenneth Caster) for financial supports.

REFERENCES

- (1) Jeon, N. J.; Noh, J. H.; Yang, W. S.; Kim, Y. C.; Ryu, S.; Seo, J.; Seok, S. I. Compositional Engineering of Perovskite Materials for High-Performance Solar Cells. *Nature* **2015**, *517*, 476–480.
- (2) Tan, H.; Jain, A.; Voznyy, O.; Lan, X.; García de Arquer, F. P.; Fan, J. Z.; Quintero-Bermudez, R.; Yuan, M.; Zhang, B.; Zhao, Y.; Fan, F.; Li, P.; Quan, L. N.; Zhao, Y.; Lu, Z. H.; Yang, Z.; Hoogland, S.; Sargent, E. H. Efficient and Stable Solution-Processed Planar Perovskite Solar Cells via Contact Passivation. *Science* **2017**, 355, 722–726.
- (3) Stranks, S. D.; Eperon, G. E.; Grancini, G.; Menelaou, C.; Alcocer, M. J.; Leijtens, T.; Herz, L. M.; Petrozza, A.; Snaith, H. J. Electron-Hole Diffusion Lengths Exceeding 1 Micrometer in an Organometal Trihalide Perovskite Absorber. *Science* **2013**, 342, 341–344
- (4) Yang, W. S.; Park, B. W.; Jung, E. H.; Jeon, N. J.; Kim, Y. C.; Lee, D. U.; Shin, S. S.; Seo, J.; Kim, E. K.; Noh, J. H.; Seok, S. I. Iodide Management in Formamidinium-Lead-Halide—based Perovskite Layers for Efficient Solar Cells. *Science* **2017**, *356*, 1376—1379.
- (Ś) Bi, D.; Yi, C.; Luo, J.; Décoppet, J.-D.; Zhang, F.; Zakeeruddin, S. M.; Li, X.; Hagfeldt, A.; Grätzel, M. Polymer-Templated Nucleation and Crystal Growth of Perovskite Films for Solar Cells with Efficiency Greater than 21%. *Nat. Energy* **2016**, *1*, No. 16142.
- (6) https://www.nrel.gov/pv/assets/pdfs/best-research-cell-efficiencies.20190802.pdf.
- (7) Hou, Y.; Aydin, E.; Bastiani, M. D.; Xiao, C. X.; Isikgor, F. H.; Xue, D.; Chen, J.; Chen, B.; Bahrami, H. B.; Chowdhury, A. H.; Johnston, A.; Baek, S. W.; Huang, Z. R.; Wei, M. Y.; Dong, Y. T.; Troughton, J.; Jalmood, R.; Mirabelli, A. J.; Allen, T. G.; Kerschaver, E. V.; Saidaminov, M. I.; Baran, D.; Qiao, Q. Q.; Zhu, K.; Sargent, E. H.; De Wolf, S. Efficient Tandem Solar Cells with Solution-Processed Perovskite on Textured Crystalline Silicon. *Science* **2020**, *367*, 1135—1140.
- (8) Nie, W.; Tsai, H.; Asadpour, R.; Blancon, J.-C.; Neukirch, A. J.; Gupta, G.; Crochet, J. J.; Chhowalla, M.; Tretiak, S.; Alam, M. A.; et al. High-Efficiency Solution-Processed Perovskite Solar Cells with Millimeter-Scale Grains. *Science* **2015**, 347, 522–525.
- (9) Tsai, H. H.; Nie, W. Y.; Blancon, J. C.; Toumpos, C. C. S.; Asadpour, R.; Harutyunyan, B.; Neukirch, A. J.; Verduzco, R.; Crochet, J. J.; Tretiak, S.; Pedesseau, L.; Even, J.; Alam, M. A.; Gupta, G.; Lou, J.; Ajayan, P. M.; Bedzyk, M. J.; Kanatzidis, M. G.; Mohite, A. D. High-Efficiency Two-Dimensional Ruddlesden—Popper Perovskite Solar Cells. *Nature* **2016**, *536*, 312—316.
- (10) Jung, E. H.; Jeon, N. J.; Park, E. Y.; Moon, C. S.; Shin, T. J.; Yang, T. Y.; Noh, J. H.; Seo, J. Efficient, Stable and Scalable Perovskite Solar Cells Using Poly(3-hexylthiophene). *Nature* **2019**, 567, 511–515.
- (11) Park, N. G. Perovskite Solar Cells: an Emerging Photovoltaic Technology. *Mater. Today* **2015**, *18*, 65–72.
- (12) Edri, E.; Kirmayer, S.; Henning, A.; Mukhopadhyay, S.; Gartsman, K.; Rosenwaks, Y.; Hodes, G.; Cahen, D. Why Lead Methylammonium Triiodide Perovskite-Based Solar Cells Require a Mesoporous Electron Transporting Scaffold (but not Necessarily a Hole Conductor). *Nano Lett.* **2014**, *14*, 1000–1004.

- (13) Wolff, C. M.; Caprioglio, P.; Stolterfoht, M.; Neher, D. Nonradiative Recombination in Perovskite Solar Cells: the Role of Interfaces. *Adv. Mater.* **2019**. *31*. No. 1902762.
- (14) Jiang, Q.; Zhao, Y.; Zhang, X. W.; Yang, X. L.; Chen, Y.; Chu, Z. M.; Ye, Q. F.; Li, X. X.; Yin, Z. G.; You, J. B. Surface Passivation of Perovskite Film for Efficient Solar Cells. *Nat. Photonics* **2019**, *13*, 500–504.
- (15) Zheng, X. P.; Chen, B.; Dai, J.; Fang, Y. J.; Bai, Y.; Lin, Y. Z.; Wei, H. T.; Zeng, X. C.; Huang, J. S. Defect passivation in Hybrid Perovskite Solar Cells Using Quaternary Ammonium Halide Anions and Cations. *Nat. Energy* **2017**, *2*, No. 17102.
- (16) Xu, J.; Buin, A.; Ip, A. H.; Li, W.; Voznyy, O.; Comin, R.; Yuan, M.; Jeon, S.; Ning, Z.; Mcdowell, J. J.; Sargent, E. H.; et al. Perovskite—Fullerene Hybrid Materials Suppress Hysteresis in Planar Diodes. *Nat. Commun.* **2015**, *6*, No. 7081.
- (17) Fu, S.; Li, X. D.; Wan, L.; Wu, Y. L.; Zhang, W. X.; Wang, Y. M.; Bao, Q. Y.; Fang, J. F. Efficient Passivation with Lead Pyridine-2-Carboxylic for High-Performance and Stable Perovskite Solar Cells. *Adv. Energy Mater.* **2019**, *9*, No. 1901852.
- (18) Gao, F.; Zhao, Y.; Zhang, X. W.; You, J. B. Recent Progresses on Defects toward Efficient Perovskite Solar Cells. *Adv. Energy Mater.* **2020**, *10*, No. 1902650.
- (19) Yoon, S. J.; Kuno, M.; Kamat, P. V. How Halide Ion Defects Influence Photoinduced Segregation in Mixed Halide Perovskites. *ACS Energy Lett.* **2017**, *2*, 1507–1514.
- (20) Lee, J. W.; Kim, H. S.; Park, N. G. Lewis Acid—Base Adduct Approach for High Efficiency Perovskite Solar Cells. *Acc. Chem. Res.* **2016**, *49*, 311–319.
- (21) Zhang, F.; Bi, D. Q.; Pellet, N. C.; Xiao, X.; Li, Z.; Berry, J. J.; Zakeeruddin, S. M.; Zhu, K.; Gratzel, M. Suppressing Defects through the Synergistic Effect of a Lewis Base and a Lewis Acid for Highly Efficient and Stable Perovskite Solar Cells. *Energy Environ. Sci.* 2018, 11, 3480–3490.
- (22) Luo, J. S.; Xia, J. X.; Yang, H.; Chen, L. L.; Wan, Z. Q.; Han, F.; Malik, H. A.; Zhu, X. H.; Jia, C. Y. Toward High-Efficiency, Hysteresis-Less, Stable Perovskite Solar Cells: Unusual Doping of a Hole-Transporting Material Using a Fluorine-Containing Hydrophobic Lewis Acid. *Energy Environ. Sci.* 2018, 11, 2035–2045.
- (23) Li, B.; Zhang, Y. A.; Fu, L.; Yu, T.; Zhou, S. J.; Zhang, L. Y.; Yin, L. W. Surface Passivation Engineering Strategy to Fully-Inorganic Cubic CsPbI₃ Perovskites for High-Performance Solar Cells. *Nat. Commun.* 2018, 9, No. 1076.
- (24) Wang, K.; Liu, C.; Yi, C.; Chen, L.; Zhu, J. H.; Weiss, R. A.; Gong, X. Hybrid Solar Cells: Efficient Perovskite Hybrid Solar Cells via Ionomer Interfacial Engineering. *Adv. Funct. Mater.* **2015**, 25, 6875–6884.
- (25) Kim, M.; Motti, S. G.; Sorrentino, R.; Petrozza, A. Enhanced Solar Cell Stability by Hygroscopic Polymer Passivation of Metal Halide Perovskite Thin Film. *Energy Environ. Sci.* **2018**, *11*, 2609–2619
- (26) Lu, J.; Chen, S.-C.; Zheng, Q. Defect Passivation of CsPbIBr₂ Perovskites For High-Performance Solar Cells with Large Open-Circuit Voltage of 1.28 V. ACS Appl. Energy Mater. **2018**, *1*, 5872–5878.
- (27) You, Y.; Tian, W.; Wang, M.; Cao, F.; Sun, H.; Li, L. PEG Modified CsPbIBr₂ Perovskite Film for Efficient and Stable Solar Cells. *Adv. Mater. Interfaces* **2020**, *7*, No. 2000537.
- (28) Niu, T. Q.; Lu, J.; Munir, R.; Li, J. B.; Barrit, D.; Zhang, X.; Hu, H. L.; Yang, Z.; Amassian, A.; Zhao, K.; Liu, S. Z. Stable High-Performance Perovskite Solar Cells via Grain Boundary Passivation. *Adv. Mater.* **2018**, *30*, No. 1706576.
- (29) Zhao, T.; Chueh, C. C.; Chen, Q.; Rajagopal, A.; Jen, A. K. Y. Inorganic Hybrid Perovskites by Diammonium Iodide toward High-Performance Photovoltaic Devices. ACS Energy Lett. 2016, 1, 757–763
- (30) Xu, W.; Zheng, L.; Zhang, X.; Cao, Y.; Meng, T.; Wu, D.; Liu, L.; Hu, W.; Gong, X. Efficient Perovskite Solar Cells Fabricated by Co Partially Substituted Hybrid Perovskite. *Adv. Energy Mater.* **2018**, *8*, No. 1703178.

- (31) Bi, C.; Wang, Q.; Shao, Y.; Yuan, Y.; Xiao, Z.; Huang, J. Non-Wetting Surface-Driven High-Aspect-Ratio Crystalline Grain Growth For Efficient Hybrid Perovskite Solar Cells. *Nat. Commun.* **2015**, *6*, No. 7747.
- (32) Shao, Y.; Fang, Y.; Li, T.; Dong, Q. F.; Deng, Y. H.; Gruverman, A.; Shielda, J.; Huang, J. S.; Wang, Q.; et al. Grain Boundary Dominated Ion Migration in Polycrystalline Organic-Inorganic Halide Perovskite Films. *Energy Environ. Sci.* **2016**, *9*, 1752–1759.
- (33) Wang, K.; Zheng, L. Y.; Zhu, T.; Liu, L.; Becker, M. L.; Gong, X. High Performance Perovskites Solar Cells by Hybrid Perovskites Co-Crystallized with Poly(ethylene oxide). *Nano Energy* **2020**, *67*, No. 104229.
- (34) Wang, Q.; Lyu, M. Q.; Zhang, M.; Yun, J. H.; Chen, H. J.; Wang, L. Z. Transition from the Tetragonal to Cubic Phase of Organohalide Perovskite: The Role of Chlorine in Crystal Formation of CH₃NH₃PbI₃ on TiO₂ Substrates. *J. Phys. Chem. Lett.* **2015**, *6*, 4379–4384.
- (35) Zhang, T. Y.; Guo, N. J.; Li, G.; Qian, X. F.; Zhao, Y. X. A Controllable Fabrication of Grain Boundary PbI₂ Nanoplates Passivated Lead Halide Perovskites for High Performance Solar Cells. *Nano Energy* **2016**, *26*, 50–56.
- (36) Zheng, L. Y.; Mukherjee, S.; Wang, K.; Hay, M. E.; Boudouris, B. W.; Gong, X. Radical Polymers as Interfacial Layers in Inverted Hybrid Perovskite Solar Cells. *J. Mater. Chem. A* **2017**, *5*, 23831–23839.
- (37) Wang, K.; Zheng, L.; Zhu, T.; Yao, X.; Yi, C.; Zhang, X.; Cao, Y.; Liu, L.; Hu, W.; Gong, X. Efficient Perovskite Solar Cells by Hybrid Perovskites Incorporated with Heterovalent Neodymium Cations. *Nano Energy* **2019**, *61*, 352–360.
- (38) Seifter, J.; Sun, Y.; Choi, H.; Lee, B. H.; Nguyen, T. L.; Woo, H. Y.; Heeger, A. J. Measurement of the Charge Carrier Mobility Distribution in Bulk Heterojunction Solar Cells. *Adv. Mater.* **2015**, *27*, 4989–4996.
- (39) Zhu, T.; Zheng, L. Y.; Xiao, Z.; Meng, X. Y.; Liu, L.; Ding, L. M.; Gong, X. Functionality of Non-Fullerene Electron Acceptors in Ternary Organic Solar Cells. *Sol. RRL* **2019**, *3*, No. 1900322.
- (40) Gonzalez-Pedro, V.; Juarez-Perez, E. J.; Arsyad, W. S.; Barea, E. M.; Fabregat-Santiago, F.; Mora-Sero, I.; Bisquert, J. General Working Principles of CH₃NH₃PbX₃ Perovskite Solar Cells. *Nano Lett.* **2014**, *14*, 888–893.
- (41) Wang, K.; Yi, C.; Liu, C.; Hu, X. W.; Chuang, S.; Gong, X. Effects of Magnetic Nanoparticles and External Magnetostatic Field on the Bulk Heterojunction Polymer Solar Cells. *Sci. Rep.* **2015**, *5*, No. 9265.
- (42) Itoh, E.; Nakagoshi, S. Impedance Analysis of the Multilayered Organic Solar Cells with and without Hole Buffer Layer. *Jpn. J. Appl. Phys.* **2014**, *53*, No. 04ER15.
- (43) Cowan, S. R.; Banerji, N.; Leong, W. L.; Heeger, A. J. Charge Formation, Recombination, and Sweep-Out Dynamics in Organic Solar Cells. *Adv. Funct. Mater.* **2012**, 22, 1116–1128.
- (44) Cowan, S. R.; Street, R.; Cho, S.; Heeger, A. Transient Photoconductivity in Polymer Bulk Heterojunction Solar Cells: Competition between Sweep-Out and Recombination. *Phys. Rev. B* **2011**, *83*, No. 035205.
- (45) Bube, R. H. Trap Density Determination by Space-Charge-Limited Currents. J. Appl. Phys. 1962, 33, 1733-1737.
- (46) Murgatroyd, P. N. Theory of Space-Charge-Limited Current Enhanced by Frenkel Effect. J. Phys. D Appl. Phys. 1970, 3, 151.
- (47) Kim, H.-S.; Park, N.-G. Parameters Affecting I–V Hysteresis of CH₃NH₃PbI₃ Perovskite Solar Cells: Effects of Perovskite Crystal Size and Mesoporous TiO₂ Layer. *J. Phys. Chem. Lett.* **2014**, *5*, 2927–2934.
- (48) Yoon, H.; Kang, S. M.; Lee, J. K.; Choi, M. Hysteresis-Free Low-Temperature-Processed Planar Perovskite Solar Cells with 19.1% Efficiency. *Energy Environ. Sci.* **2016**, *9*, 2262–2266.
- (49) Wang, K.; Liu, C.; Du, P. C.; Zheng, J.; Gong, X. Bulk Heterojunction Perovskite Hybrid Solar Cells with Large Fill Factor. *Energy Environ. Sci.* **2015**, *8*, 1245–1255.

- (50) Hu, X. W.; Yi, C.; Wang, M.; Hsu, C. H.; Zhang, K.; Zhong, C. M.; Huang, F.; Gong, X.; Cao, Y.; et al. Performance Inverted Organic Photovoltaics with Over 1- μ m Thick Active Layers. *Adv. Energy Mater.* **2014**, *4*, No. 1400378.
- (51) Liu, C.; Wang, K.; Du, P. C.; Meng, T. Y.; Yu, X. F.; Cheng, S. Z. D.; Gong, X. High Performance Planar Heterojunction Perovskite Solar Cells with Fullerene Derivatives as the Electron Transport Layer. ACS Appl. Mater. Interfaces 2015, 7, 1153–1159.
- (52) Liu, C.; Wang, K.; Yi, C.; Shi, X. J.; Smith, A. W.; Gong, X.; Heeger, A. J. Efficient Perovskite Hybrid Photovoltaics via Alcohol-Vapor Annealing Treatment. *Adv. Funct. Mater.* **2016**, *26*, 101–110.